APPLIED SCIENCES AND ENGINEERING

Origami by frontal photopolymerization

Zeang Zhao,[1,2]* Jiangtao Wu,[2]* Xiaoming Mu,[2] Haosen Chen,[3] H. Jerry Qi,[2]† Daining Fang[1,3]†

Origami structures are of great interest in microelectronics, soft actuators, mechanical metamaterials, and biomedical devices. Current methods of fabricating origami structures still have several limitations, such as complex material systems or tedious processing steps. We present a simple approach for creating three-dimensional (3D) origami structures by the frontal photopolymerization method, which can be easily implemented by using a commercial projector. The concept of our method is based on the volume shrinkage during photopolymerization. By adding photoabsorbers into the polymer resin, an attenuated light field is created and leads to a nonuniform curing along the thickness direction. The layer directly exposed to light cures faster than the next layer; this nonuniform curing degree leads to nonuniform curing–induced volume shrinkage. This further introduces a nonuniform stress field, which drives the film to bend toward the newly formed side. The degree of bending can be controlled by adjusting the gray scale and the irradiation time, an easy approach for creating origami structures. The behavior is examined both experimentally and theoretically. Two methods are also proposed to create different types of 3D origami structures.

INTRODUCTION

Three-dimensional (3D) origami structures are of great interest in microelectronics (*1*), soft sensors and actuators (*2*), mechanical metamaterials (*3*), and biomedical devices (*4*). Over the past few years, different self-folding origami strategies were proposed, which have further broadened the potential application fields for origami structures. One popular approach is to use functional materials that have self-actuation behavior, such as thermal response (*5*, *6*), light activation (*7*–*9*), and chemical sensitivity (*10*, *11*). These materials transform into different shapes under specific stimulus. Another common method of self-folding relies on the large volume change of polymers during swelling and deswelling. Complex 3D structures can be created through a spatial control over the swelling property (*12*, *13*). Some researchers have also introduced mechanical loads to guide the origami bending process, such as capillary force (*14*), gas flow (*15*), delamination-induced buckling (*16*), and the deformation of the substrate (*17*). However, several limitations still exist, such as complex material system or structure design, and relatively tedious fabrication process.

Frontal photopolymerization (FPP) (*18*, *19*) is a process in which a polymer film is continuously cured from one side in a thick layer of liquid resin. In the presence of strong light attenuation, the solidification front initiates at the surface upon illumination and propagates toward the liquid side as the irradiation time increases. The process can be delicately tuned by controlling the illumination time and the light intensity, and the method has been used to fabricate microfluidic devices (*20*) and the synthesis of microparticles (*21*).

Here, we show that, without cumbersome processing steps, origami structures can be created using the FPP method with conventional photocurable polymers, and the origami process is almost spontaneous instead of a response to external stimulus. Several other methods of light stimuli–responsive origami could be found in some recent reviews (*22*, *23*). The concept of our method is based on photopolymerization-induced volume shrinkage. During photopolymerization of the resin, the material volume decreases as a result of covalent bond formation between monomers and cross-linkers (*24*). This behavior is commonly assumed to be undesirable in additive manufacturing (or 3D printing) (*25*, *26*), microfabrication (*27*), and manufacturing of polymer composites (*28*), because it causes shape distortion and internal stress. However, in FPP, the moving front of a cured region leads to a nonuniform volume shrinkage, which can be controlled and used to create bending structures and 3D origami shapes. The process is shown schematically in Fig. 1A, which is similar to a digital light processing (DLP) 3D printing approach (*29*), where a light is projected upward from the bottom through a transparent substrate to cure the liquid resin. To control light penetration, we added photoabsorbers to induce an intensity gradient in the resin. Note that light intensity is continuous, but the mechanism of forming origami bending can be better explained by using the layer concept. Upon irradiation, the layer directly exposed to light will be cured immediately, whereas the resin adjacent to this layer, without sufficient illumination, still remains in the liquid state. As the front of liquid-solid transition propagates through the liquid resin, the thickness of the cured polymer film increases. Due to the presence of a light intensity gradient caused by the photoabsorber, volume shrinkage happens in a sequential manner. That is, early cured layer shrinks first, but because the connection between the cured material and the substrate is not fully established, there is not much internal stress developed and the first layer can be considered stress-free, whereas subsequently cured layer shrinks under the confinement of the early cured layer. The phenomenon is very similar to the shape distortion in layer-by-layer stereolithography (*26*), but here, the sample is continuous instead of laminated. As a result, a nonuniform stress field develops across the sample's thickness, where the early cured layer (near the substrate) has a compressive stress and the newly cured layer has a tensile stress. At this moment, the sample has a tendency to bend toward the newly cured material. Because of the restriction from the substrate, the film has an internal stress gradient but remains flat in shape. Once the film is moved from the substrate, to release the internal stress, residual compressive stress drives the material to expand, whereas residual tensile stress drives the material to contract, and the sample bends toward the newly cured side. The bending curvature is related to several processing conditions, such as light intensity and illumination time. By imposing spatial control over the curing condition, complex 3D origami structures can be created. It should be noted that, compared with some recent

[1]College of Engineering, Peking University, Beijing 100871, P. R. China. [2]George W. Woodruff School of Mechanical Engineering, Georgia Institute of Technology, Atlanta, GA 30332, USA. [3]Institute of Advanced Structure Technology, Beijing Institute of Technology, Beijing 100081, P. R. China.
*These authors contributed equally to this work.
†Corresponding author. Email: qih@me.gatech.edu (H.J.Q.); fangdn@pku.edu.cn or fangdn@bit.edu.cn (D.F.)

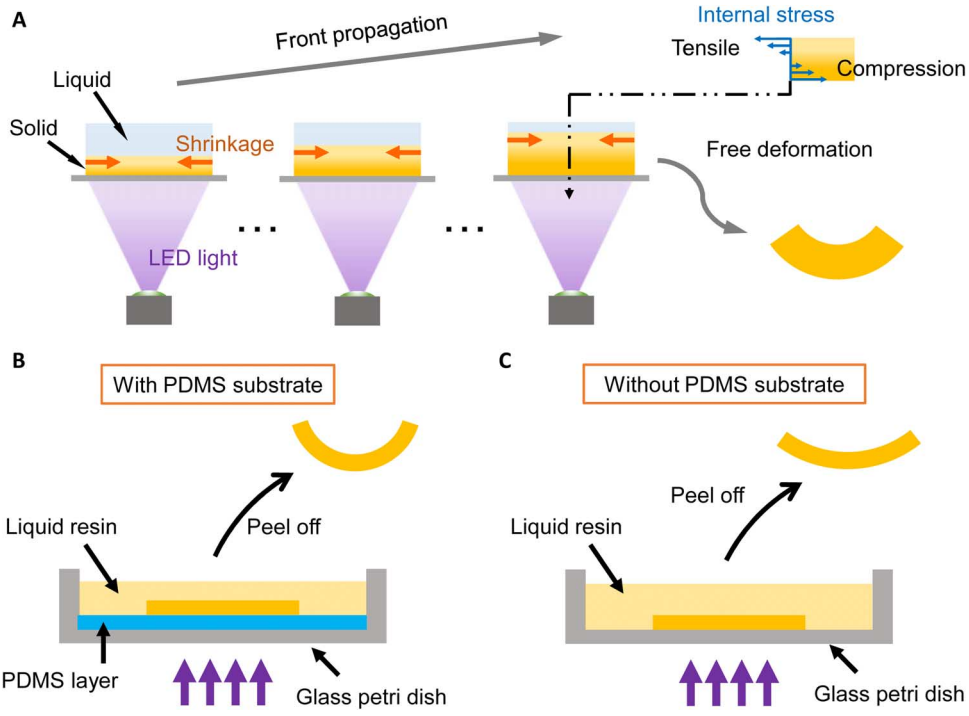

Fig. 1. Shrinkage-induced bending during FPP. (**A**) Schematic process of volume shrinkage–induced bending: Sequential shrinkage occurs during the FPP of a polymer sheet, and the internal stress developed during the process drives the sheet to bend. LED, light-emitting diode. (**B**) Schematic process of shrinkage-induced bending test (with PDMS substrate). (**C**) Schematic process of shrinkage-induced bending test (without PDMS substrate).

published works on 3D shape formed by the DLP approach (*30*, *31*), the method in this paper has the advantage of the elimination of external stimulus.

RESULTS

Shrinkage-induced bending

The FPP process was proved by attenuated total reflection Fourier transform infrared (FT-IR) spectrum on the top and bottom surface of the samples cured by irradiation (light intensity, 5 mW cm^{-2}) from the bottom. Experimental results summarized in fig. S1 show that (i) there is a significant gradient of photopolymerization degree across sample thickness and (ii) the front of photopolymerization transfers continuously with the irradiation time. Detailed discussions can be found in the Supplementary Materials. The curing property of acrylate resin was characterized by testing the photopolymerized thin films (0.05 mm) with different illumination times under a constant intensity of 5 mW cm^{-2}, and the results are also shown in the Supplementary Materials. As shown in fig. S2B, the Young's modulus of the sample increases nearly linearly with the normalized conversion degree φ of C=C double bonds. Note here that the fully cured resin does not pass its glass transition; therefore, the Young's modulus shows a nearly linear functions of degree of conversion; this relationship would become highly nonlinear once the glass transition is passed. Significant shrinkage strain around 5% occurred after solidification, and its variation became much milder as the reaction proceeded (fig. S2C). During FPP (for example, the continuous growth of a polymer film in fig. S2D), the evolution of these two properties can be combined to control the development of the internal stress field.

To demonstrate the concept of shrinkage-induced bending, we cured polymer strips in a glass petri dish filled with liquid resin, where the light was projected upward from the bottom. Inspired by the antistiction effect from both residual oxygen inhibition (*32*) and pendent oligomers at the surface (*33*) of poly(dimethylsiloxane) (PDMS), we inserted a PDMS substrate to make sure that cured parts would not stick to the petri dish so that the sample could be easily removed. The process is shown schematically in Fig. 1B. After different periods of irradiation under various light intensities, the solidified strip was moved out of the liquid to measure its bending curvature. Figure 2A shows some selected samples that were cured under a light intensity of 5 mW cm^{-2}. Sample thickness increases with irradiation time, which is similar to the result in fig. S2D. The bending curvatures were measured from several figures similar to Fig. 2A (at least four figures for each condition) and are summarized in Fig. 2B with symbols. Note that the curvature decreases with both illumination time and incident light intensity. Although the sequential shrinkage behavior remains the same, bending stiffness increases because of the increased thickness and modulus, making it more difficult to bend. Bending almost disappears when the curing time is longer than 10 s under an intensity of 9.5 mW cm^{-2}. Under different intensities, the tendencies of time-dependent curvature reduction are nearly identical, but they differ in the decay speed. Figure 2B was redrawn in fig. S3 by changing axis x to the irradiation dose (irradiation time × incident light intensity). Results under different intensities coincide into a single curve, and this indicates that bending curvature is solely dependent on the incident energy dose during reaction.

For a comparison group, the PDMS substrate in the petri dish was removed, and then rectangular strips were cured in the same manner with an incident intensity of 5 mW cm^{-2} (Fig. 1C). The results are shown by red open circles in Fig. 2B. In this case, the bottom material, which was cured the earliest, adhered to the substrate and could not shrink freely. After the part was cured and peeled off from the substrate, the bottom surface shrinks slightly to release internal stress. This tendency

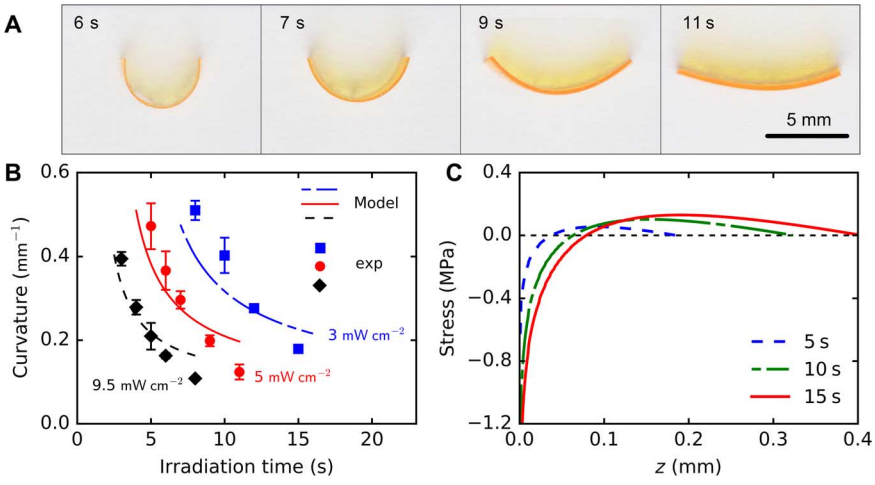

Fig. 2. Experimental results of shrinkage-induced bending. (**A**) Rectangular samples cured in a petri dish with different irradiation times (light intensity, 5 mW cm^{-2}). (**B**) Bending curvature of photopolymerized strips as a function of irradiation time and incident light intensity. (**C**) Stress distribution across sample thickness (light intensity, 5 mW cm^{-2}).

is in contrast to the fact that the bottom part is compressed during the sequential shrinkage process, and therefore, the overall bending curvature is reduced. Thus, the boundary condition at the interface between the substrate and the cured resin plays a key role in determining the shape-changing behaviors. The effect of the surface layer's confinement becomes negligible when the total thickness of the cured sample increases, because the overall stress gradient along the thickness direction governs the bending behavior.

The shrinkage-induced bending is described by a theoretical model based on beam theory (*34*). During photopolymerization, samples are constrained by liquid resin. The out-plane rotation is restricted, and only in-plane stretching occurs. The mechanical behavior of films under illumination should be governed by force equilibrium along the thickness direction

$$\int_0^{\tilde{z}(t)} \sigma dz = \int_0^{\tilde{z}(t)} E(\varepsilon - \varepsilon^S) dz = 0 \quad (1)$$

Here, $\tilde{z}$ is the solidified thickness. The stress σ is decided by $\sigma = E\varepsilon^e = E(\varepsilon - \varepsilon^s)$, where E is the Young's modulus and ε^e, ε, and ε^s are the elastic strain, the total strain, and the shrinkage strain, respectively. Both E and ε^s are dependent on the conversion degree φ of double bonds in the acrylate resin (details of the photopolymerization model can be found in the Supplementary Materials). The total strain ε and shrinkage strain ε^s are set to zero if the conversion degree φ is below the gel point φ_c. Note that the integral domain of Eq. 1 varies with time. Thus, it is solved incrementally by time intervals to obtain the value of ε at different z and t.

When the solidified film is removed from the substrate, the constraint disappears, and the part will bend under its internal stress field. Both force equilibrium and moment equilibrium should be satisfied

$$\int_0^{\tilde{z}(t)} \sigma dz = \int_0^{\tilde{z}(t)} E\varepsilon^e dz = 0 \quad (2A)$$

$$\int_0^{\tilde{z}(t)} z\sigma dz = \int_0^{\tilde{z}(t)} zE\varepsilon^e dz = 0 \quad (2B)$$

Here, the elastic strain is obtained by a superposition of bending and stretching (*5*)

$$\varepsilon^e = \varepsilon - \varepsilon^S + \varepsilon_b + \kappa\left(z - \frac{\tilde{z}}{2}\right) \quad (3)$$

where ε_b is the bending strain of the midplane at $z = \tilde{z}/2$, and κ is the bending curvature. The value of ε for in-plane stretching is obtained from the calculation of Eq. 1. Equation 2A and B can be solved as a whole to get the value of ε_b and κ.

Theoretical calculation results based on the model are shown in Fig. 2B in lines. The dependence of the curvature κ on the irradiation time and the light intensity is captured well. Discrepancies between experiments and theoretical results may come from our rather simplified model, which may not be able to capture every detail of the complicated chemical-mechanical coupling during FPP. Nonetheless, this model can offer some insight into the deformation mechanism and help design. An interesting finding is that, as a result of more uniform intensity distribution and higher rate of thickness increase, the decrease of curvature with irradiation time is faster under a stronger incident light. This observation leads to a design concept wherein, by varying light intensity (or grayscale pattern) in a 2D illumination pattern, we can create thick stiff panels or soft thin bending parts: For the same light irradiation time, parts under high light intensity have high stiffness but less bending, and parts under low light intensity are relatively soft but with a sufficient bending curvature. When compared according to irradiation dose (fig. S3), modeling results for different intensities also coincide into a single curve. This is an intrinsic feature of the model, because incident light intensity (I_0) and irradiation time (t) contribute equally in the reaction kinetics (eq. S3).

On the basis of Eq. 1 in the model, the evolution of the stress field for a sample cured under irradiation of 5 mW cm^{-2} is shown in Fig. 2C. The bottom layer that is cured first stays in a compressive state, whereas the top part is in tension. The absolute value of stress is higher in the bottom part, as a result of high modulus and accumulation of the sequential shrinkage. However, the overall curvature decreases with the

increase of irradiation time. This is because the thickness and modulus of the cured sample become sufficiently larger to resist bending deformation; the slightly higher stress near the bottom layer is not enough to compensate the bending stiffness. As a result, when the irradiation time is long, the bending is actually small.

Origami structures created by one-side illumination

Using the shrinkage-induced bending in photopolymerization, we can create complex 3D structures from flat polymer sheets with programmed 2D light patterns. It should be pointed out that, if the polymer sheet is cured by illumination from the bottom, as we explained before, then it can only bend toward the top side. We will show first how to produce origami structures from this type of one-side illumination. With the projector, 2D light patterns with spatial control over intensity are created through variation of the gray scale. Low light intensity is used at those points, where significant bending is expected. For the table structure in Fig. 3 (A to D), intensities were set to 15 and 3 mW cm^{-2} for the panel and legs, respectively. This was realized by creating figures with a spatial variation of gray scale (inset in Fig. 3A). The correlation between the gray-scale value and the light intensity was determined experimentally and can be found in fig. S4. After a specific irradiation time (10 s for Fig. 3A), as discussed before, the cured sheet remained flat on the substrate. Parts that were exposed to high intensity were thicker, and parts that were exposed to low intensity (for example, those legs in Fig. 3A) were relatively thinner. When the sample was removed from the liquid, those parts that were exposed to low intensity (legs in Fig. 3B) bent toward the newly formed side as a result of nonuniform stress. Because the bending parts had a lower stiffness, this configuration was not stable. To fix the shape, we held the samples using tweezers and further cured them under a uniform light of 10 mW cm^{-2} for 20 to 30 s (Fig. 3C), which stiffened the structure due to the marked increase of the modulus in the previously soft parts. After this post-curing, the sample became strong enough to support some weight. A table structure holding several glass coverslips (with a total weight of 1.1 g, which is about 13 times the weight of the table) is shown in Fig. 3D.

Much more elegant control over the light pattern produces structures with higher complexity. Flowers with different opening degrees are shown in Fig. 3E. These four flowers were all created using an irradiation period of 6 s. The illumination intensity of the central round panel was 10 mW cm^{-2}, and petal intensities were set to 2.5, 4, 6, and 7 mW cm^{-2}. The sample that was illuminated with the lowest intensity shows the smallest opening angle. The round panel at the center was illuminated with a high intensity, and it remained flat in all four cases. A polymer sheet with continuous variation of bending curvature is shown

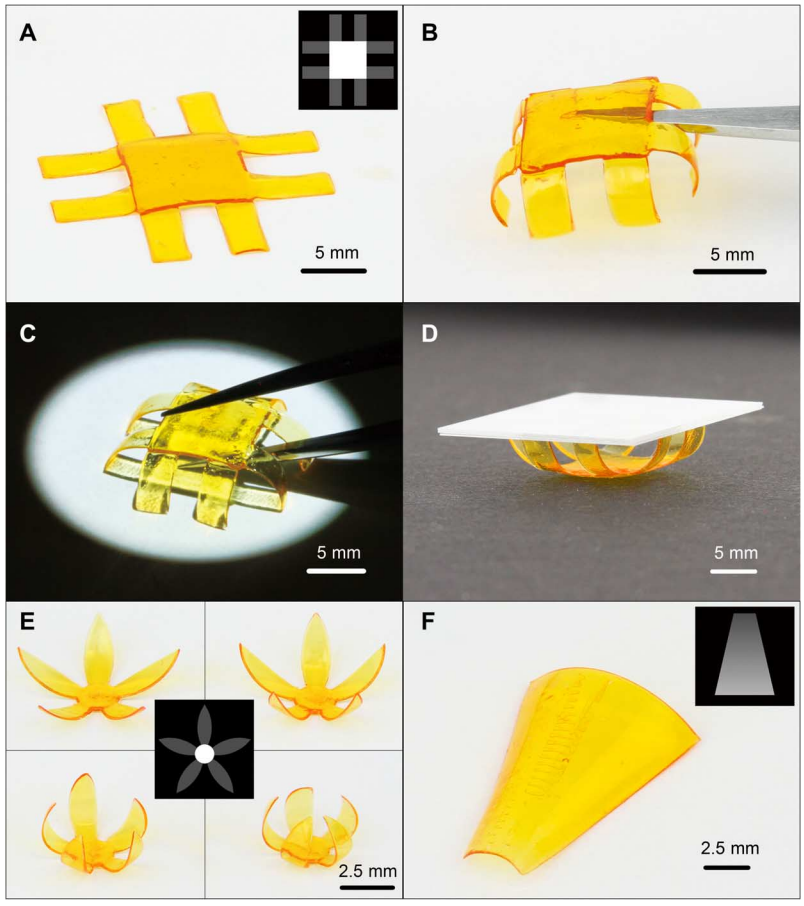

Fig. 3. Fabrication of origami structures by one-side illumination. (**A**) Polymer sheet right after photopolymerization (panel intensity, 15 mW cm^{-2}; leg intensity, 3 mW cm^{-2}; irradiation time, 10 s). (**B**) Free bending of spatial, differently cured sheet. (**C**) Shape fixing of bending structures by post-curing (under a uniform light of 10 mW cm^{-2} for 20 to 30 s). (**D**) Sample after post-curing is stiff and able to hold several glass coverslips. (**E**) Flower structures with different opening degrees (panel intensity, 10 mW cm^{-2}; petal intensities, 2.5, 4, 6, and 7 mW cm^{-2} for different opening degrees; irradiation time, 6 s). (**F**) Polymer sheet with a continuous variation of curvature (intensity varied from 2.5 to 10 mW cm^{-2}; irradiation time, 4 s). Insets in (A), (E), and (F) indicate the light patterns.

in Fig. 3F. This structure was realized by illuminating a trapezoidal pattern with a gradient of gray scale for 4 s. The edge with the highest curvature was illuminated with the lowest intensity (2.5 mW cm^{-2}), and intensity gradually increased to the other edge (to 10 mW cm^{-2}).

3D bending structures were created by using a combination of flat panels and hinges bent toward one side. Some different types of polyhedron capsules are shown in Fig. 4. To stabilize the bending process, we introduced extra panels in the light pattern. For example, to form the shape in Fig. 4A, we attached four more panels marked by a red "x" to the net pattern of octahedron in Fig. 4B. During the bending process, an extra panel overlapped on the top of a neighbor panel and thus stabilized the structure. The overlapped panels stuck together after post-curing of the residual resin at the surface.

Origami structures created by two-side illumination

Structures presented in the previous section were created by polymer sheets bending toward one single side; thus, the freedom of design is limited. In this section, we show a modified method that is able to create more complex origami structures. The process is shown schematically in Fig. 5A. Liquid resin was injected into a flat mold confined by two glass slides; two PDMS anti-stiction layers were pasted on the inner sides of the glass slides to avoid adhesion of cured parts. On the basis of the FPP growth dynamics in fig. S2D and the evolution of curvature in Fig. 2B, the distance between the two PDMS slides was confined to 0.5 mm. In the first step, parts designed to bend toward direction 1 (indicated by number 1 in Fig. 5A) were illuminated under low intensity from the bottom. After that, the whole structure was flipped over without in-plane movement of position. Then, parts designed to bend toward direction 2 (indicated by number 2 in Fig. 5A) were illuminated in the same manner. By releasing the mold, the cured sheet bent toward the two different sides. In a real application, one can apply two light sources or use a light splitter to expedite the processing time. Two light patterns can be projected in sequence to realize this two-step illumination. The positions marked by 2 could be made black during the first illumination, and the positions marked by 1 could be made black during the second illumination, whereas plane panels could be irradiated in both steps.

3D origami structures produced by two-side illumination are presented in Fig. 5 (B to E). Figure 5B shows a table with legs in two directions, created by illuminating the leg parts from two sides. The intersection points of different hinges were left as voids to facilitate the bending process. This is shown, for example, by the vertices in the Miura structure (Fig. 5C) and the top of a pyramid tent (Fig. 5D). Different intensities can be used for separate hinges to enrich the freedom of the origami. For the origami crane in Fig. 5E, an intensity of 2 mW cm^{-2} was used for the wing hinges, and a very low intensity of 1 mW cm^{-2} was used for the hinges of legs and tails.

A comparison between these two methods shows that they are suitable for different conditions. Although the second method of two-side illumination has the ability to create very complex structures, extra processing steps become inevitable, such as, for example, the preparation of a mold and the insertion of liquid resin. As for the one-side method, structures can be created by just shining a single pattern onto a liquid resin vat, but the degree of freedom of the origami is confined. Thus, if a structure can be designed simply by a combination of hinges turned toward one direction, then the one-side method is sufficient. The two-side illumination method becomes necessary when more delicate control over the origami is desired. Note that, in both methods, because the flat shapes were frontal photopolymerized with in-plane variations of incident light intensity, the final thickness may not be uniform everywhere.

CONCLUSION

We presented a method to create 3D origami structures from photocurable acrylate resin. The origami bending process is based on volume

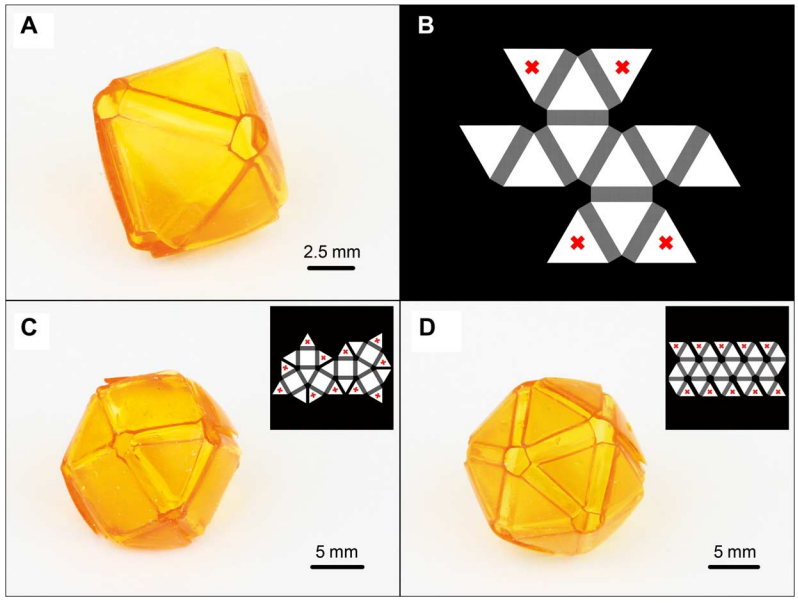

Fig. 4. Polyhedrons created by one-side illumination. (**A**) Octahedron (panel intensity, 15 mW cm^{-2}; hinge intensity, 3 mW cm^{-2}; irradiation time, 6 s). (**B**) Grayscale pattern of octahedron structure. (**C**) Truncated cube (panel intensity, 15 mW cm^{-2}; hinge intensity, 3.3 mW cm^{-2}; irradiation time, 6 s). (**D**) Regular icosahedron (panel intensity, 15 mW cm^{-2}; hinge intensity, 4 mW cm^{-2}; irradiation time, 6 s). Insets in (C) and (D) indicate the corresponding light patterns, and the red x indicates that the panel is an extra one used for stabilizing the structure.

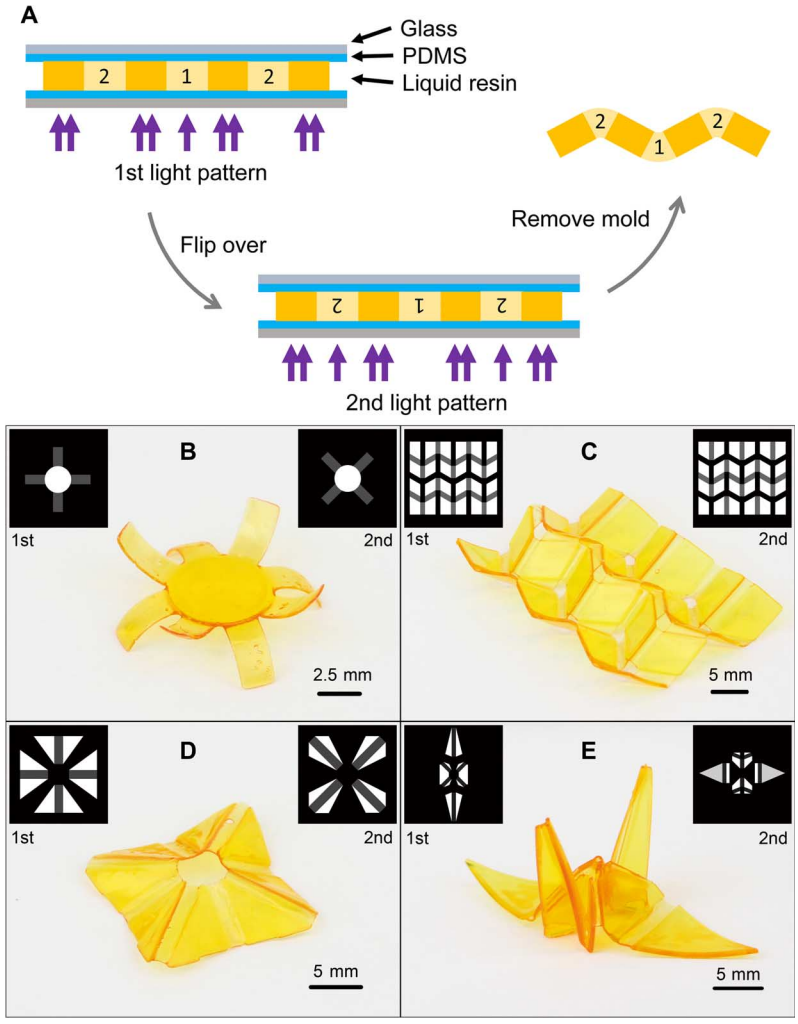

Fig. 5. Fabrication of origami structures by two-side illuminations. (**A**) Schematic process of two-side illumination method. (**B**) Table (panel intensity, 18 mW cm^{-2}; petal intensity, 2.5 mW cm^{-2}; irradiation time of each side, 7 s). (**C**) Miura structure (panel intensity, 20 mW cm^{-2}; hinge intensity, 2 mW cm^{-2}; irradiation time of each side, 7 s). (**D**) Tent (panel intensity, 18 mW cm^{-2}; hinge intensity, 2 mW cm^{-2}; irradiation time of each side, 7 s). (**E**) Crane (panel intensity, 20 mW cm^{-2}; body hinge intensity, 1 mW cm^{-2}; wing hinge intensity, 2 mW cm^{-2}; irradiation time of each side, 15 s). Created by two-side illumination method.

shrinkage during the photopolymerization of liquid resin. When a polymer film is gradually photopolymerized from one side, the initially cured material shrinks freely to release internal stress, whereas newly cured material shrinks under the confinement of old material. A nonuniform stress field appears in the process, with a tendency to drive the film to bend toward the newly formed side. This behavior was investigated in detail through systematic experiments. We found that the bending curvature induced by sequential shrinkage decreases with both irradiation time and illumination light intensity. A simple theoretical model was developed to describe the buildup of internal stress and the evolution of bending curvature. On the basis of experiment, observation, and theoretical analysis, two separate methods were developed to create 3D origami structures. The first method, one-side illumination, is suitable for structures combined with parts bending toward one direction. The second method, which has a more delicate control over the bending process, can be used for structures with hinges bending toward two directions. These methods provide a new and simple route for creating origami-based metamaterials and the 2D-to-3D fabrication of electronic devices.

MATERIALS AND METHODS

The liquid resin used in this work was a mixture of 99.28 weight % (wt %) PEGDA [poly(ethylene glycol) (700) diacrylate; Sigma-Aldrich], 0.67 wt % photoinitiator Irgacure 819 [phenylbis(2,4,6-trimethylbenzoyl) phosphine oxide; Sigma-Aldrich], and 0.05 wt % photoabsorber Sudan I (Sigma-Aldrich), which is the same as that used in 3D printing (*35*). An ultraviolet (UV)–visible light projector (wavelength, 200 to 1000 nm; model D912HD, Vivitek USA; with the UV filter removed by B9Creations) was used as a light source. Light intensity was measured by a radiometer (IL1400A, International Light Technologies). To investigate the curing behavior of our resin, we used a component with the same ratio of PEGDA and photoinitiator as mentioned above, whereas the photoabsorber was removed. Films (0.05 mm thick) were cured between glass slides for different time periods with an irradiation intensity of 1.5 mW cm^{-2}. The material properties of the thin film were considered uniform due to limited light attenuation. The conversion of double bonds in the film was measured by FT-IR spectrum on an FT-IR spectrometer (Nicolet iS50, Thermo Scientific). The Young's modulus of

the film was measured on a dynamic mechanical analysis tester (Q800, TA Instruments). The mass density was obtained by a pycnometer (AccuPyc II 1340, Micromeritics), which can accurately measure the volume of a specific mass through gas displacement. For each irradiation time, the FT-IR test, the mechanical test, and the mass density test were conducted on a same batch of sample. To investigate the effect of curing time and intensity on shrinkage-induced bending, we performed another set of experiments by pouring liquid resin into a glass petri dish, with a 0.5-mm-thick layer of transparent PDMS (Sylgard 184, Dow Corning Corporation) as a substrate to preclude adhesion of cured parts. After that, a light pattern of a small rectangle was projected to the center of the resin from the bottom. The thickness and bending curvature of the cured rectangular strip were measured in ImageJ (*36*) as functions of illumination time and intensity. For the comparison group, the PDMS layer was removed so that the bottoms of the cured samples would stick to the glass substrate. The illumination condition was maintained by measuring the light intensity at the top of an empty petri dish with or without the PDMS substrate.

SUPPLEMENTARY MATERIALS

Supplementary material for this article is available at http://advances.sciencemag.org/cgi/content/full/3/4/e1602326/DC1

Supplementary Text

fig. S1. Conversion profile of frontal photopolymerized samples.

fig. S2. Properties of the resin during photopolymerization.

fig. S3. Bending curvature as a function of irradiation dose.

fig. S4. Relation between light intensity and gray scale.

movie S1. Bending of an octahedron guided by tweezers.

movie S2. Bending of an origami crane guided by tweezers.

References (*37*–*39*)

REFERENCES AND NOTES

1. J. Rogers, Y. G. Huang, O. G. Schmidt, D. H. Gracias, Origami MEMS and NEMS. *MRS Bull.* **41**, 123–129 (2016).
2. Z. Chen, G. S. Huang, I. Trase, X. M. Han, Y. F. Mei, Mechanical self-assembly of a strain-engineered flexible layer: Wrinkling, rolling, and twisting. *Phys. Rev. Applied* **5**, 017001 (2016).
3. L. H. Dudte, E. Vouga, T. Tachi, L. Mahadevan, Programming curvature using origami tessellations. *Nat. Mater.* **15**, 583–588 (2016).
4. R. Fernandes, D. H. Gracias, Self-folding polymeric containers for encapsulation and delivery of drugs. *Adv. Drug Deliv. Rev.* **64**, 1579–1589 (2012).
5. Q. Ge, C. K. Dunn, H. J. Qi, M. L. Dunn, Active origami by 4D printing. *Smart Mater. Struct.* **23**, 094007 (2014).
6. S. M. Felton, M. T. Tolley, B. Shin, C. D. Onal, E. D. Demaine, D. Rus, R. J. Wood, Self-folding with shape memory composites. *Soft Matter* **9**, 7688–7694 (2013).
7. T. H. Ware, M. E. McConney, J. J. Wie, V. P. Tondiglia, T. J. White, Voxelated liquid crystal elastomers. *Science* **347**, 982–984 (2015).
8. J. Ryu, M. D'Amato, X. D. Cui, K. N. Long, H. J. Qi, M. L. Dunn, Photo-origami—Bending and folding polymers with light. *Appl. Phys. Lett.* **100**, 161908 (2012).
9. X. Mu, N. Sowan, J. A. Tumbic, C. N. Bowman, P. T. Mather, H. J. Qi, Photo-induced bending in a light-activated polymer laminated composite. *Soft Matter* **11**, 2673–2682 (2015).
10. H. Meng, G. Q. Li, A review of stimuli-responsive shape memory polymer composites. *Polymer* **54**, 2199–2221 (2013).
11. T. G. Leong, C. L. Randall, B. R. Benson, N. Bassik, G. M. Stern, D. H. Gracias, Tetherless thermobiochemically actuated microgrippers. *Proc. Natl. Acad. Sci. U.S.A.* **106**, 703–708 (2009).
12. A. S. Gladman, E. A. Matsumoto, R. G. Nuzzo, L. Mahadevan, J. A. Lewis, Biomimetic 4D printing. *Nat. Mater.* **15**, 413–418 (2016).
13. J.-H. Na, A. A. Evans, J. Bae, M. C. Chiappelli, C. D. Santangelo, R. J. Lang, T. C. Hull, R. C. Hayward, Programming reversibly self-folding origami with micropatterned photo-crosslinkable polymer trilayers. *Adv. Mater.* **27**, 79–85 (2015).
14. C. Py, P. Reverdy, L. Doppler, J. Bico, B. Roman, C. N. Baroud, Capillary origami: Spontaneous wrapping of a droplet with an elastic sheet. *Phys. Rev. Lett.* **98**, 156103 (2007).
15. F. Ilievski, A. D. Mazzeo, R. E. Shepherd, X. Chen, G. M. Whitesides, Soft robotics for chemists. *Angew. Chem. Int. Ed. Engl.* **50**, 1890–1895 (2011).
16. S. Edmondson, K. Frieda, J. E. Comrie, P. R. Onck, W. T. S. Huck, Buckling in quasi-2D polymers. *Adv. Mater.* **18**, 724–728 (2006).
17. Z. Yan, F. Zhang, J. Wang, F. Liu, X. Guo, K. Nan, Q. Lin, M. Gao, D. Xiao, Y. Shi, Controlled mechanical buckling for origami-inspired construction of 3D microstructures in advanced materials. *Adv. Funct. Mater.* **26**, 2629–2639 (2016).
18. A. Vitale, M. G. Hennessy, O. K. Matar, J. T. Cabral, A unified approach for patterning via frontal photopolymerization. *Adv. Mater.* **27**, 6118–6124 (2015).
19. J. T. Cabral, S. D. Hudson, C. Harrison, J. F. Douglas, Frontal photopolymerization for microfluidic applications. *Langmuir* **20**, 10020–10029 (2004).
20. C. Harrison, J. T. Cabral, C. M. Stafford, A. Karim, E. J. Amis, A rapid prototyping technique for the fabrication of solvent-resistant structures. *J. Micromech. Microeng.* **14**, 153–158 (2004).
21. D. Dendukuri, D. C. Pregibon, J. Collins, T. A. Hatton, P. S. Doyle, Continuous-flow lithography for high-throughput microparticle synthesis. *Nat. Mater.* **5**, 365–369 (2006).
22. Y. Liu, J. Genzer, M. D. Dickey, "2D or not 2D": Shape-programming polymer sheets. *Prog. Polym. Sci.* **52**, 79–106 (2016).
23. D. H. Gracias, Stimuli responsive self-folding using thin polymer films. *Curr. Opin. Chem. Eng.* **2**, 112–119 (2013).
24. C. N. Bowman, C. J. Kloxin, Toward an enhanced understanding and implementation of photopolymerization reactions. *AIChE J.* **54**, 2775–2795 (2008).
25. D. Karalekas, A. Aggelopoulos, Study of shrinkage strains in a stereolithography cured acrylic photopolymer resin. *J. Mater. Process. Tech.* **136**, 146–150 (2003).
26. Y.-M. Huang, C.-P. Jiang, Curl distortion analysis during photopolymerisation of stereolithography using dynamic finite element method. *Int. J. Adv. Manuf. Technol.* **21**, 586–595 (2003).
27. A. Amirsadeghi, J. J. Lee, S. Park, A simulation study on the effect of cross-linking agent concentration for defect tolerant demolding in UV nanoimprint lithography. *Langmuir* **28**, 11546–11554 (2012).
28. J. M. Svanberg, J. A. Holmberg, Prediction of shape distortions Part I. FE-implementation of a path dependent constitutive model. *Composites Part A* **35**, 711–721 (2004).
29. X. Zheng, H. Lee, T. H. Weisgraber, M. Shustef, J. DeOtte, E. B. Duoss, J. D. Kuntz, M. M. Biener, Q. Ge, J. A. Jackson, S. O. Kucheyev, N. X. Fang, C. M. Spadaccini, Ultralight, ultrastiff mechanical metamaterials. *Science* **344**, 1373–1377 (2014).
30. L. Huang, R. Jiang, J. Wu, J. Song, H. Bai, B. Li, Q. Zhao, T. Xie, Ultrafast digital printing toward 4D shape changing materials. *Adv. Mater.* **29**, 1605390 (2017).
31. Z. Zhao, J. Wu, X. Mu, H. Chen, H. J. Qi, D. Fang, Desolvation induced origami of photocurable polymers by digit light processing. *Macromol. Rapid Commun.* **2016**, 1600625 (2016).
32. D. Dendukuri, P. Panda, R. Haghgooie, J. M. Kim, T. A. Hatton, P. S. Doyle, Modeling of oxygen-inhibited free radical photopolymerization in a PDMS microfluidic device. *Macromolecules* **41**, 8547–8556 (2008).
33. L. J. T. Landherr, C. Cohen, L. A. Archer, Effect of pendent chains on the interfacial properties of thin polydimethylsiloxane (PDMS) networks. *Langmuir* **27**, 5944–5952 (2011).
34. S. Timoshenko, Analysis of bi-metal thermostats. *J. Opt. Soc. Am.* **11**, 233–255 (1925).
35. M. P. Lee, G. J. T. Cooper, T. Hinkley, G. M. Gibson, M. J. Padgett, L. Cronin, Development of a 3D printer using scanning projection stereolithography. *Sci. Rep.* **5**, 9857 (2015).
36. C. A. Schneider, W. S. Rasband, K. W. Eliceiri, NIH Image to ImageJ: 25 years of image analysis. *Nat. Methods* **9**, 671–675 (2012).
37. D. Adolf, J. E. Martin, Time cure superposition during cross-linking. *Macromolecules* **23**, 3700–3704 (1990).
38. G. Socrates, *Infrared and Raman Characteristic Group Frequencies: Tables and Charts* (John Wiley & Sons, 2004).
39. M. Sangermano, S. Marchi, L. Valentini, S. B. Bon, P. Fabbri, Transparent and conductive graphene oxide/poly(ethylene glycol) diacrylate coatings obtained by photopolymerization. *Macromol. Mater. Eng.* **296**, 401–407 (2011).

Acknowledgments

Funding: We acknowledge the support of the NSF award (CMMI-1462894, CMMI-1462895, and EFRI-1435452). We also acknowledge the support of an Air Force Office of Scientific Research grant (15RT0885). Z.Z. acknowledges support from Chinese Scholarship Council (201506010219). **Author contributions:** Z.Z. and J.W. conducted the experiments with the help of X.M. Z.Z. and H.C. led the theoretical modeling. H.J.Q. and D.F. contributed to the concept development and manuscript writing. All authors reviewed the manuscript. **Competing interests:** All authors declare that they have no competing interests. **Data and materials availability:** All data needed to evaluate the conclusions in the paper are present in the paper and/or the Supplementary Materials. Additional data related to this paper may be requested from the authors.

Submitted 22 September 2016
Accepted 23 February 2017
Published 28 April 2017
10.1126/sciadv.1602326

Citation: Z. Zhao, J. Wu, X. Mu, H. Chen, H. J. Qi, D. Fang, Origami by frontal photopolymerization. *Sci. Adv.* **3**, e1602326 (2017).

ScienceAdvances
AAAS

Origami by frontal photopolymerization
Zeang Zhao, Jiangtao Wu, Xiaoming Mu, Haosen Chen, H. Jerry Qi and Daining Fang (April 28, 2017)
Sci Adv 2017, 3:.
doi: 10.1126/sciadv.1602326